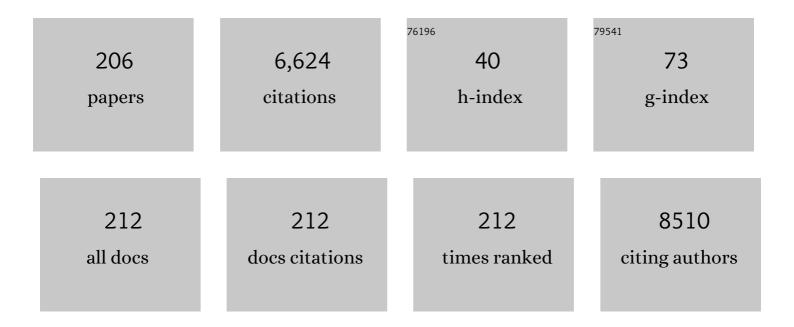
List of Publications by Year in descending order

Source: https://exaly.com/author-pdf/5424598/publications.pdf Version: 2024-02-01



#	Article	IF	CITATIONS
1	Not-so-supervised: A survey of semi-supervised, multi-instance, and transfer learning in medical image analysis. Medical Image Analysis, 2019, 54, 280-296.	7.0	545
2	Evaluation of Registration Methods on Thoracic CT: The EMPIRE10 Challenge. IEEE Transactions on Medical Imaging, 2011, 30, 1901-1920.	5.4	363
3	Quantitative Analysis of Pulmonary Emphysema Using Local Binary Patterns. IEEE Transactions on Medical Imaging, 2010, 29, 559-569.	5.4	319
4	A Genome-Wide Association Study Identifies Five Loci Influencing Facial Morphology in Europeans. PLoS Genetics, 2012, 8, e1002932.	1.5	274
5	Machine learning approaches in medical image analysis: From detection to diagnosis. Medical Image Analysis, 2016, 33, 94-97.	7.0	231
6	PRAGMA-CF. A Quantitative Structural Lung Disease Computed Tomography Outcome in Young Children with Cystic Fibrosis. American Journal of Respiratory and Critical Care Medicine, 2015, 191, 1158-1165.	2.5	192
7	Transfer Learning Improves Supervised Image Segmentation Across Imaging Protocols. IEEE Transactions on Medical Imaging, 2015, 34, 1018-1030.	5.4	191
8	MRBrainS Challenge: Online Evaluation Framework for Brain Image Segmentation in 3T MRI Scans. Computational Intelligence and Neuroscience, 2015, 2015, 1-16.	1.1	179
9	Extraction of Airways From CT (EXACT'09). IEEE Transactions on Medical Imaging, 2012, 31, 2093-2107.	5.4	173
10	Gray Matter Age Prediction as a Biomarker for Risk of Dementia. Proceedings of the National Academy of Sciences of the United States of America, 2019, 116, 21213-21218.	3.3	147
11	2D–3D shape reconstruction of the distal femur from stereo X-ray imaging using statistical shape models. Medical Image Analysis, 2011, 15, 840-850.	7.0	139
12	Combining Generative and Discriminative Representation Learning for Lung CT Analysis With Convolutional Restricted Boltzmann Machines. IEEE Transactions on Medical Imaging, 2016, 35, 1262-1272.	5.4	116
13	Vessel-guided airway tree segmentation: A voxel classification approach. Medical Image Analysis, 2010, 14, 527-538.	7.0	112
14	Interactive segmentation of abdominal aortic aneurysms in CTA images. Medical Image Analysis, 2004, 8, 127-138.	7.0	105
15	Adapting Active Shape Models for 3D Segmentation of Tubular Structures in Medical Images. Lecture Notes in Computer Science, 2003, 18, 136-147.	1.0	97
16	Semi-supervised Medical Image Segmentation via Learning Consistency Under Transformations. Lecture Notes in Computer Science, 2019, , 810-818.	1.0	91
17	Three-Dimensional Carotid Ultrasound Plaque Texture Predicts Vascular Events. Stroke, 2014, 45, 2695-2701.	1.0	83
18	Cystic Fibrosis: Are Volumetric Ultra-Low-Dose Expiratory CT Scans Sufficient for Monitoring Related Lung Disease?. Radiology, 2009, 253, 223-229.	3.6	82

#	Article	IF	CITATIONS
19	High shear stress relates to intraplaque haemorrhage in asymptomatic carotid plaques. Atherosclerosis, 2016, 251, 348-354.	0.4	79
20	Texture-Based Analysis of COPD: A Data-Driven Approach. IEEE Transactions on Medical Imaging, 2012, 31, 70-78.	5.4	78
21	Enlarged perivascular spaces in brain MRI: Automated quantification in four regions. NeuroImage, 2019, 185, 534-544.	2.1	77
22	Short-term effect of changes in smoking behaviour on emphysema quantification by CT. Thorax, 2011, 66, 55-60.	2.7	70
23	Mass preserving image registration for lung CT. Medical Image Analysis, 2012, 16, 786-795.	7.0	67
24	Transfer Learning for Image Segmentation by Combining Image Weighting and Kernel Learning. IEEE Transactions on Medical Imaging, 2019, 38, 213-224.	5.4	66
25	A Texton-Based Approach for the Classification of Lung Parenchyma in CT Images. Lecture Notes in Computer Science, 2010, 13, 595-602.	1.0	63
26	Developing and validating COVID-19 adverse outcome risk prediction models from a bi-national European cohort of 5594 patients. Scientific Reports, 2021, 11, 3246.	1.6	62
27	Transfer Learning for Multicenter Classification of Chronic Obstructive Pulmonary Disease. IEEE Journal of Biomedical and Health Informatics, 2018, 22, 1486-1496.	3.9	57
28	Quantitative vertebral morphometry using neighbor-conditional shape models. Medical Image Analysis, 2007, 11, 503-512.	7.0	55
29	Chest Computed Tomography Scores Are Predictive of Survival in Patients with Cystic Fibrosis Awaiting Lung Transplantation. American Journal of Respiratory and Critical Care Medicine, 2012, 185, 1096-1103.	2.5	55
30	Diagnosis of bronchiectasis and airway wall thickening in children with cystic fibrosis: Objective airway-artery quantification. European Radiology, 2017, 27, 4680-4689.	2.3	55
31	Automated Brain Structure Segmentation Based on Atlas Registration and Appearance Models. IEEE Transactions on Medical Imaging, 2012, 31, 276-286.	5.4	54
32	Hippocampal shape is predictive for the development of dementia in a normal, elderly population. Human Brain Mapping, 2014, 35, 2359-2371.	1.9	52
33	Robust Shape Regression for Supervised Vessel Segmentation and its Application to Coronary Segmentation in CTA. IEEE Transactions on Medical Imaging, 2011, 30, 1974-1986.	5.4	51
34	Automated 3D segmentation and diameter measurement of the thoracic aorta on non-contrast enhanced CT. European Radiology, 2019, 29, 4613-4623.	2.3	45
35	Multicentre chest computed tomography standardisation in children and adolescents with cystic fibrosis: the way forward. European Respiratory Journal, 2016, 47, 1706-1717.	3.1	44
36	Toward automatic regional analysis of pulmonary function using inspiration and expiration thoracic CT. Medical Physics, 2012, 39, 1650-1662.	1.6	43

#	Article	IF	CITATIONS
37	Statistical coronary motion models for 2D+t/3D registration of X-ray coronary angiography and CTA. Medical Image Analysis, 2013, 17, 698-709.	7.0	42
38	Lung MRI and impairment of diaphragmatic function in Pompe disease. BMC Pulmonary Medicine, 2015, 15, 54.	0.8	42
39	Visual assessment of early emphysema and interstitial abnormalities on CT is useful in lung cancer risk analysis. European Radiology, 2016, 26, 487-494.	2.3	42
40	3D regression neural network for the quantification of enlarged perivascular spaces in brain MRI. Medical Image Analysis, 2019, 51, 89-100.	7.0	42
41	Relation between wall shear stress and carotid artery wall thickening MRI versus CFD. Journal of Biomechanics, 2016, 49, 735-741.	0.9	41
42	Spirometer-controlled cine magnetic resonance imaging used to diagnose tracheobronchomalacia in paediatric patients. European Respiratory Journal, 2014, 43, 115-124.	3.1	40
43	Learning Cross-Modality Representations From Multi-Modal Images. IEEE Transactions on Medical Imaging, 2019, 38, 638-648.	5.4	40
44	Toward a Theory of Statistical Tree-Shape Analysis. IEEE Transactions on Pattern Analysis and Machine Intelligence, 2013, 35, 2008-2021.	9.7	39
45	Automatic airway–artery analysis on lung CT to quantify airway wall thickening and bronchiectasis. Medical Physics, 2016, 43, 5736-5744.	1.6	38
46	Weight Preserving Image Registration for Monitoring Disease Progression in Lung CT. Lecture Notes in Computer Science, 2008, 11, 863-870.	1.0	37
47	Chest computed tomography: a validated surrogate endpoint of cystic fibrosis lung disease?. European Respiratory Journal, 2013, 42, 844-857.	3.1	36
48	Adversarial attack vulnerability of medical image analysis systems: Unexplored factors. Medical Image Analysis, 2021, 73, 102141.	7.0	35
49	Evaluation of automated statistical shape model based knee kinematics from biplane fluoroscopy. Journal of Biomechanics, 2014, 47, 122-129.	0.9	34
50	Why Does Synthesized Data Improve Multi-sequence Classification?. Lecture Notes in Computer Science, 2015, , 531-538.	1.0	34
51	Active-shape-model-based segmentation of abdominal aortic aneurysms in CTA images. , 2002, , .		30
52	Quantification of Diaphragm Mechanics in Pompe Disease Using Dynamic 3D MRI. PLoS ONE, 2016, 11, e0158912.	1.1	30
53	Image segmentation by shape particle filtering. , 2004, , .		29
54	Carotid Artery Wall Segmentation in Multispectral MRI by Coupled Optimal Surface Graph Cuts. IEEE Transactions on Medical Imaging, 2016, 35, 901-911.	5.4	29

#	Article	IF	CITATIONS
55	Optimal surface segmentation using flow lines to quantify airway abnormalities in chronic obstructive pulmonary disease. Medical Image Analysis, 2014, 18, 531-541.	7.0	28
56	Multi-Center MRI Carotid Plaque Component Segmentation Using Feature Normalization and Transfer Learning. IEEE Transactions on Medical Imaging, 2015, 34, 1294-1305.	5.4	28
57	Texture Classification in Lung CT Using Local Binary Patterns. Lecture Notes in Computer Science, 2008, 11, 934-941.	1.0	28
58	Weakly supervised object detection with 2D and 3D regression neural networks. Medical Image Analysis, 2020, 65, 101767.	7.0	27
59	A Joint 3D UNet-Graph Neural Network-Based Method for Airway Segmentation from Chest CTs. Lecture Notes in Computer Science, 2019, , 583-591.	1.0	27
60	Shape Particle Filtering for Image Segmentation. Lecture Notes in Computer Science, 2004, , 168-175.	1.0	27
61	Classification of COPD with Multiple Instance Learning. , 2014, , .		25
62	Atherosclerotic Plaque Component Segmentation in Combined Carotid MRI and CTA Data Incorporating Class Label Uncertainty. PLoS ONE, 2014, 9, e94840.	1.1	25
63	Objective airway artery dimensions compared to CT scoring methods assessing structural cystic fibrosis lung disease. Journal of Cystic Fibrosis, 2017, 16, 116-123.	0.3	25
64	Multi-atlas image registration of clinical data with automated quality assessment using ventricle segmentation. Medical Image Analysis, 2020, 63, 101698.	7.0	25
65	Weighting training images by maximizing distribution similarity for supervised segmentation across scanners. Medical Image Analysis, 2015, 24, 245-254.	7.0	23
66	Optimal Graph Based Segmentation Using Flow Lines with Application to Airway Wall Segmentation. Lecture Notes in Computer Science, 2011, 22, 49-60.	1.0	23
67	Tree-Space Statistics and Approximations for Large-Scale Analysis of Anatomical Trees. Lecture Notes in Computer Science, 2013, 23, 74-85.	1.0	23
68	Factors influencing the decline in lung density in a Danish lung cancer screening cohort. European Respiratory Journal, 2012, 40, 1142-1148.	3.1	22
69	Reversibility of trapped air on chest computed tomography in cystic fibrosis patients. European Journal of Radiology, 2015, 84, 1184-1190.	1.2	22
70	Chronic Obstructive Pulmonary Disease Quantification Using CT Texture Analysis and Densitometry: Results From the Danish Lung Cancer Screening Trial. American Journal of Roentgenology, 2020, 214, 1269-1279.	1.0	22
71	Semiautomatic Segmentation of Vertebrae in Lateral X-rays Using a Conditional Shape Model. Academic Radiology, 2007, 14, 1156-1165.	1.3	21
72	Regression-Based Cardiac Motion Prediction From Single-Phase CTA. IEEE Transactions on Medical Imaging, 2012, 31, 1311-1325.	5.4	21

#	Article	IF	CITATIONS
73	Statistical Shape Model-Based Femur Kinematics From Biplane Fluoroscopy. IEEE Transactions on Medical Imaging, 2012, 31, 1573-1583.	5.4	21
74	lmaging of respiratory muscles in neuromuscular disease: A review. Neuromuscular Disorders, 2018, 28, 246-256.	0.3	21
75	Airway tapering: an objective image biomarker for bronchiectasis. European Radiology, 2020, 30, 2703-2711.	2.3	19
76	The development of bronchiectasis on chest computed tomography in children with cystic fibrosis: can pre-stages be identified?. European Radiology, 2016, 26, 4563-4569.	2.3	18
77	Airway Tree Extraction with Locally Optimal Paths. Lecture Notes in Computer Science, 2009, 12, 51-58.	1.0	18
78	A computer aided detection system for cerebral microbleeds in brain MRI. , 2012, , .		17
79	Geodesic Atlas-Based Labeling of Anatomical Trees: Application and Evaluation on Airways Extracted From CT. IEEE Transactions on Medical Imaging, 2015, 34, 1212-1226.	5.4	17
80	Automatic emphysema detection using weakly labeled HRCT lung images. PLoS ONE, 2018, 13, e0205397.	1.1	17
81	Vessel tree extraction using locally optimal paths. , 2010, , .		16
82	Learning Features for Tissue Classification with the Classification Restricted Boltzmann Machine. Lecture Notes in Computer Science, 2014, , 47-58.	1.0	16
83	Effect of inspiration on airway dimensions measured in maximal inspiration CT images of subjects without airflow limitation. European Radiology, 2014, 24, 2319-2325.	2.3	16
84	A Hierarchical Scheme for Geodesic Anatomical Labeling of Airway Trees. Lecture Notes in Computer Science, 2012, 15, 147-155.	1.0	16
85	An end-to-end approach to segmentation in medical images with CNN and posterior-CRF. Medical Image Analysis, 2022, 76, 102311.	7.0	16
86	Deep learning methods for automatic evaluation of delayed enhancement-MRI. The results of the EMIDEC challenge. Medical Image Analysis, 2022, 79, 102428.	7.0	16
87	Cerebellum segmentation in MRI using atlas registration and local multi-scale image descriptors. , 2009, , .		15
88	Graph refinement based airway extraction using mean-field networks and graph neural networks. Medical Image Analysis, 2020, 64, 101751.	7.0	15
89	Early Experiences with Crowdsourcing Airway Annotations in Chest CT. Lecture Notes in Computer Science, 2016, , 209-218.	1.0	15
90	Image Dissimilarity-Based Quantification of Lung Disease from CT. Lecture Notes in Computer Science, 2010, 13, 37-44.	1.0	15

#	Article	IF	CITATIONS
91	Geometries on Spaces of Treelike Shapes. Lecture Notes in Computer Science, 2011, , 160-173.	1.0	15
92	Multi-object tracking of human spermatozoa. , 2008, , .		14
93	Automated measurement of local white matter lesion volume. NeuroImage, 2012, 59, 3901-3908.	2.1	14
94	Automatic airway segmentation from computed tomography using robust and efficient 3-D convolutional neural networks. Scientific Reports, 2021, 11, 16001.	1.6	14
95	Three-Section Expiratory CT: Insufficient for Trapped Air Assessment in Patients with Cystic Fibrosis?. Radiology, 2012, 262, 969-976.	3.6	13
96	Classification of Volumetric Images Using Multi-Instance Learning and Extreme Value Theorem. IEEE Transactions on Medical Imaging, 2020, 39, 854-865.	5.4	13
97	Automated Lesion Detection byÂRegressing Intensity-Based Distance withÂa Neural Network. Lecture Notes in Computer Science, 2019, , 234-242.	1.0	13
98	Automated Brain-Tissue Segmentation by Multi-Feature SVM Classification. , 2013, , .		13
99	Early diagnosis of dementia based on intersubject whole-brain dissimilarities. , 2010, , .		12
100	Comparison of CT and CMR for detection and quantification of carotid artery calcification: the Rotterdam Study. Journal of Cardiovascular Magnetic Resonance, 2016, 19, 28.	1.6	12
101	Three-dimensional ultrasound evaluation of the effects of pomegranate therapy on carotid plaque texture using locality preserving projection. Computer Methods and Programs in Biomedicine, 2020, 184, 105276.	2.6	12
102	Quantitative Vertebral Morphometry Using Neighbor-Conditional Shape Models. Lecture Notes in Computer Science, 2006, 9, 1-8.	1.0	12
103	Distribution, size, shape, growth potential and extent of abdominal aortic calcified deposits predict mortality in postmenopausal women. BMC Cardiovascular Disorders, 2010, 10, 56.	0.7	11
104	Multi-feature-based plaque characterization in <i>ex vivo</i> MRI trained by registration to 3D histology. Physics in Medicine and Biology, 2012, 57, 241-256.	1.6	11
105	Maximization of regional probabilities using Optimal Surface Graphs: Application to carotid artery segmentation in MRI. Medical Physics, 2018, 45, 1159-1169.	1.6	11
106	Longitudinal assessment of carotid plaque texture in three-dimensional ultrasound images based on semi-supervised graph-based dimensionality reduction and feature selection. Computers in Biology and Medicine, 2020, 116, 103586.	3.9	11
107	Interactive shape models. , 2003, 5032, 1206.		10

108 Model-based segmentation of abdominal aortic aneurysms in CTA images. , 2003, , .

10

#	Article	IF	CITATIONS
109	Voxel classification based airway tree segmentation. Proceedings of SPIE, 2008, , .	0.8	10
110	Deep Learning from Label Proportions for Emphysema Quantification. Lecture Notes in Computer Science, 2018, , 768-776.	1.0	10
111	Lung CT registration combining intensity, curves and surfaces. , 2010, , .		9
112	Vertebral fracture risk (VFR) score for fracture prediction in postmenopausal women. Osteoporosis International, 2011, 22, 2119-2128.	1.3	9
113	Automated Segmentation and Volume Measurement of Intracranial Internal Carotid Artery Calcification at Noncontrast CT. Radiology: Artificial Intelligence, 2021, 3, e200226.	3.0	9
114	Sleep and perivascular spaces in the middleâ€aged and elderly population. Journal of Sleep Research, 2022, 31, e13485.	1.7	9
115	Conditional Shape Models for Cardiac Motion Estimation. Lecture Notes in Computer Science, 2010, 13, 452-459.	1.0	9
116	Multi-object Segmentation Using Shape Particles. Lecture Notes in Computer Science, 2005, 19, 762-773.	1.0	8
117	Confidence of model based shape reconstruction from sparse data. , 2010, , .		8
118	Distribution, Size, and Shape of Abdominal Aortic Calcified Deposits and Their Relationship to Mortality in Postmenopausal Women. International Journal of Biomedical Imaging, 2012, 2012, 1-8.	3.0	8
119	Detecting emphysema with multiple instance learning. , 2018, , .		8
120	Reliability of computer-assisted periacetabular osteotomy using a minimally invasive approach. International Journal of Computer Assisted Radiology and Surgery, 2018, 13, 2021-2028.	1.7	8
121	The value of hippocampal volume, shape, and texture for 11-year prediction of dementia: a population-based study. Neurobiology of Aging, 2019, 81, 58-66.	1.5	8
122	A Transfer-Learning Approach to Image Segmentation Across Scanners by Maximizing Distribution Similarity. Lecture Notes in Computer Science, 2013, , 49-56.	1.0	8
123	Learning COPD Sensitive Filters in Pulmonary CT. Lecture Notes in Computer Science, 2009, 12, 699-706.	1.0	8
124	Dissimilarity-Based Multiple Instance Learning. Lecture Notes in Computer Science, 2010, , 129-138.	1.0	8
125	Geometric Tree Kernels: Classification of COPD from Airway Tree Geometry. Lecture Notes in Computer Science, 2013, 23, 171-183.	1.0	8
126	Label Stability in Multiple Instance Learning. Lecture Notes in Computer Science, 2015, , 539-546.	1.0	8

#	Article	IF	CITATIONS
127	Shape Particle Guided Tissue Classification. , 0, , .		7
128	A computer-based measure of irregularity in vertebral alignment is a BMD-independent predictor of fracture risk in postmenopausal women. Osteoporosis International, 2007, 18, 1525-1530.	1.3	7
129	Bicycle chain shape models. , 2009, , .		7
130	Quantitative analysis of airway abnormalities in CT. , 2010, , .		7
131	Supervised Image Segmentation across Scanner Protocols: A Transfer Learning Approach. Lecture Notes in Computer Science, 2012, , 160-167.	1.0	7
132	Automated segmentation of atherosclerotic histology based on pattern classification. Journal of Pathology Informatics, 2013, 4, 3.	0.8	7
133	Transfer learning by feature-space transformation: A method for Hippocampus segmentation across scanners. NeuroImage: Clinical, 2018, 20, 466-475.	1.4	7
134	Growth of the thoracic aorta in the smoking population: The Danish Lung Cancer Screening Trial. International Journal of Cardiology, 2020, 299, 276-281.	0.8	7
135	Chest MRI to diagnose early diaphragmatic weakness in Pompe disease. Orphanet Journal of Rare Diseases, 2021, 16, 21.	1.2	7
136	Carotid Artery Lumen Segmentation in 3D Free-Hand Ultrasound Images Using Surface Graph Cuts. Lecture Notes in Computer Science, 2013, 16, 542-549.	1.0	7
137	Quantification of lung abnormalities in cystic fibrosis using deep networks. , 2018, , .		7
138	Comparison of Shape Regression Methods under Landmark Position Uncertainty. Lecture Notes in Computer Science, 2011, 14, 434-441.	1.0	7
139	Measurements of the current density profile with tangential Thomson scattering in RTP. Plasma Physics and Controlled Fusion, 2001, 43, 443-468.	0.9	6
140	Localization and segmentation of aortic endografts using marker detection. IEEE Transactions on Medical Imaging, 2003, 22, 473-482.	5.4	6
141	Automated Segmentation of Abdominal Aortic Aneurysms in Multi-spectral MR Images. Lecture Notes in Computer Science, 2003, , 538-545.	1.0	6
142	Automated measurement of diagnostic angles for hip dysplasia. , 2013, , .		6
143	Reply: Excess Risk of Cancer from Computed Tomography Scan Is Small but Not So Low as to Be Incalculable. American Journal of Respiratory and Critical Care Medicine, 2015, 192, 1397-1399.	2.5	6
144	Automated Registration of Freehand B-Mode Ultrasound and Magnetic Resonance Imaging of the Carotid Arteries Based on Geometric Features. Ultrasound in Medicine and Biology, 2017, 43, 273-285.	0.7	6

#	Article	IF	CITATIONS
145	Technical challenges of quantitative chest MRI data analysis in a large cohort pediatric study. European Radiology, 2019, 29, 2770-2782.	2.3	6
146	A Cross-Center Smoothness Prior for Variational Bayesian Brain Tissue Segmentation. Lecture Notes in Computer Science, 2019, , 360-371.	1.0	6
147	Carotid Artery Wall Segmentation by Coupled Surface Graph Cuts. Lecture Notes in Computer Science, 2013, , 38-47.	1.0	6
148	Early Detection of Emphysema Progression. Lecture Notes in Computer Science, 2010, 13, 193-200.	1.0	6
149	Segmentation of Intracranial Arterial Calcification with Deeply Supervised Residual Dropout Networks. Lecture Notes in Computer Science, 2017, , 356-364.	1.0	6
150	Aorta and pulmonary artery segmentation using optimal surface graph cuts in non-contrast CT. , 2018, , .		6
151	Dissimilarity representations in lung parenchyma classification. , 2009, , .		5
152	Maximum a Posteriori Estimation of Linear Shape Variation With Application to Vertebra and Cartilage Modeling. IEEE Transactions on Medical Imaging, 2011, 30, 1514-1526.	5.4	5
153	Supervised in-vivo plaque characterization incorporating class label uncertainty. , 2012, , .		5
154	Quantification of Smoothing Requirement for 3D Optic Flow Calculation of Volumetric Images. IEEE Transactions on Image Processing, 2013, 22, 2128-2137.	6.0	5
155	Nonrigid Registration of Volumetric Images Using Ranked Order Statistics. IEEE Transactions on Medical Imaging, 2014, 33, 422-432.	5.4	5
156	Intracranial arteriosclerosis is related to cerebral small vessel disease: a prospective cohort study. Neurobiology of Aging, 2021, 105, 16-24.	1.5	5
157	Quantizing Calcification in the Lumbar Aorta on 2-D Lateral X-Ray Images. Lecture Notes in Computer Science, 2005, , 409-418.	1.0	5
158	Hydranet: Data Augmentation for Regression Neural Networks. Lecture Notes in Computer Science, 2019, , 438-446.	1.0	5
159	Quantification and Visualization of Variation in Anatomical Trees. Association for Women in Mathematics Series, 2015, , 57-79.	0.1	5
160	Assessment of fully automatic segmentation of pulmonary artery and aorta on noncontrast CT with optimal surface graph cuts. Medical Physics, 2021, 48, 7837.	1.6	5
161	A Family of Principal Component Analyses for Dealing with Outliers. Lecture Notes in Computer Science, 2007, 10, 178-185.	1.0	5
162	Multiple Classifier Systems in Texton-Based Approach for the Classification of CT Images of Lung. Lecture Notes in Computer Science, 2011, , 153-163.	1.0	5

#	Article	IF	CITATIONS
163	Dissimilarity-Based Classification of Anatomical Tree Structures. Lecture Notes in Computer Science, 2011, 22, 475-485.	1.0	5
164	Diaphragmatic dysfunction in neuromuscular disease, an MRI study. Neuromuscular Disorders, 2022, 32, 15-24.	0.3	5
165	Bronchial wall parameters on CT in healthy never-smoking, smoking, COPD, and asthma populations: a systematic review and meta-analysis. European Radiology, 2022, 32, 5308-5318.	2.3	5
166	Representation Learning for Cross-Modality Classification. Lecture Notes in Computer Science, 2017, , 126-136.	1.0	4
167	Reference values and variation of acetabular angles measured by computed tomography in 170 asymptomatic hips. Acta Radiologica, 2019, 60, 895-901.	0.5	4
168	A Pattern Classification Approach to Aorta Calcium Scoring in Radiographs. Lecture Notes in Computer Science, 2005, , 170-177.	1.0	4
169	Discriminative Shape Alignment. Lecture Notes in Computer Science, 2009, 21, 459-466.	1.0	4
170	Prediction of Dementia by Hippocampal Shape Analysis. Lecture Notes in Computer Science, 2010, , 42-49.	1.0	4
171	Shape regression for vertebra fracture quantification. , 2005, , .		3
172	Vertebral fracture classification. , 2007, , .		3
173	Plaque characterization in ex vivo MRI evaluated by dense 3D correspondence with histology. , 2011, , .		3
174	Letter by Bos et al Regarding Article, "Intracranial Carotid Calcification on Cranial Computed Tomography: Visual Scoring Methods, Semiautomated Scores, and Volume Measurements in Patients With Stroke― Stroke, 2015, 46, e254.	1.0	3
175	Spectral Data Augmentation Techniques to Quantify Lung Pathology from CT-Images. , 2020, , .		3
176	Extraction of Airways with Probabilistic State-Space Models and Bayesian Smoothing. Lecture Notes in Computer Science, 2017, , 53-63.	1.0	3
177	Quantifying Calcification in the Lumbar Aorta on X-Ray Images. Lecture Notes in Computer Science, 2007, 10, 352-359.	1.0	3
178	Quantitative Airway Analysis in Longitudinal Studies Using Groupwise Registration and 4D Optimal Surfaces. Lecture Notes in Computer Science, 2013, 16, 287-294.	1.0	3
179	Toward automated detection and segmentation of aortic calcifications from radiographs. , 2007, , .		3
180	<title>Semiautomatic aortic endograft localization for postoperative evaluation of endovascular aneurysm treatment</title> . , 2001, , .		3

#	Article	IF	CITATIONS
181	Crowdsourced Emphysema Assessment. Lecture Notes in Computer Science, 2017, , 126-135.	1.0	3
182	Region-of-Interest Guided Supervoxel Inpainting for Self-supervision. Lecture Notes in Computer Science, 2020, , 500-509.	1.0	3
183	Creating a training set for artificial intelligence from initial segmentations of airways. European Radiology Experimental, 2021, 5, 54.	1.7	3
184	Supervised shape analysis for risk assessment in osteoporosis. , 2008, , .		2
185	Mass preserving registration for lung CT. , 2009, , .		2
186	Towards exaggerated emphysema stereotypes. , 2012, , .		2
187	Shape-based Assessment of Vertebral Fracture Risk in Postmenopausal Women Using Discriminative Shape Alignment. Academic Radiology, 2012, 19, 446-454.	1.3	2
188	Local appearance features for robust MRI brain structure segmentation across scanning protocols. , 2013, , .		2
189	Cooperative carotid artery centerline extraction in MRI. PLoS ONE, 2018, 13, e0197180.	1.1	2
190	Increasing Accuracy of Optimal Surfaces Using Min-Marginal Energies. IEEE Transactions on Medical Imaging, 2019, 38, 1559-1568.	5.4	2
191	Learning to Quantify Emphysema Extent: What Labels Do We Need?. IEEE Journal of Biomedical and Health Informatics, 2020, 24, 1149-1159.	3.9	2
192	Bicycle chain shape models. , 2009, , .		2
193	Fully Automated Lung Volume Assessment from MRI in a Population-based Child Cohort Study. , 2017, , .		2
194	A pixelwise inpainting-based refinement scheme for quantizing calcification in the lumbar aorta on 2D lateral x-ray images. , 2006, 6144, 474.		1
195	Quantitative imaging biomarkers in neurologic disease: Population study perspective. , 2012, , .		1
196	Efficient nonrigid registration using ranked order statistics. , 2013, , .		1
197	Extracting tree structures in CT data by tracking multiple statistically ranked hypotheses. Medical Physics, 2019, 46, 4431-4440.	1.6	1
198	Crowdsourcing airway annotations in chest computed tomography images. PLoS ONE, 2021, 16, e0249580.	1.1	1

#	Article	IF	CITATIONS
199	Feature-Space Transformation Improves Supervised Segmentation Across Scanners. Lecture Notes in Computer Science, 2015, , 85-93.	1.0	1
200	Improved Tissue Segmentation by Including an MR Acquisition Model. Lecture Notes in Computer Science, 2011, , 152-159.	1.0	1
201	Automated Quantification of Enlarged Perivascular Spaces in Clinical Brain MRI Across Sites. Lecture Notes in Computer Science, 2019, , 103-111.	1.0	1
202	Special Issue on Tribute Workshop for Peter Johansen. Journal of Mathematical Imaging and Vision, 2008, 31, 119-120.	0.8	0
203	Integrating local voxel classification and global shape models for medical image segmentation. Proceedings of SPIE, 2008, , .	0.8	0
204	MACD: an imaging marker for cardiovascular disease. Proceedings of SPIE, 2010, , .	0.8	0
205	Comparison of ct and MRI on the detection and quantification of carotid artery calcification: The rotterdam study. Atherosclerosis, 2017, 263, e17.	0.4	0
206	MRI changes in diaphragmatic motion and curvature in Pompe disease over time. European Radiology, 0,	2.3	0